



Effect of Deformation Methods on the Accuracy of Deformable Image Registration From Kilovoltage CT to Tomotherapy Megavoltage CT

Technology in Cancer Research & Treatment
Volume 18: 1-9
© The Author(s) 2019
Article reuse guidelines:
sagepub.com/journals-permissions
DOI: 10.1177/1533033818821186
journals.sagepub.com/home/tct


Wannapha Nobnop, PhD¹ , Imjai Chitapanarux, MD¹,
Somsak Wanwilairat, PhD¹, Ekkasit Tharavichitkul, MD¹,
Vicharn Lorvidhaya, MD¹, and Patumrat Sripan, PhD¹

Abstract

Introduction: The registration accuracy of megavoltage computed tomography images is limited by low image contrast when compared to that of kilovoltage computed tomography images. Such issues may degrade the deformable image registration accuracy. This study evaluates the deformable image registration from kilovoltage to megavoltage images when using different deformation methods and assessing nasopharyngeal carcinoma patient images. **Methods:** The kilovoltage and the megavoltage images from the first day and the 20th fractions of the treatment day of 12 patients with nasopharyngeal carcinoma were used to evaluate the deformable image registration application. The deformable image registration image procedures were classified into 3 groups, including kilovoltage to kilovoltage, megavoltage to megavoltage, and kilovoltage to megavoltage. Three deformable image registration methods were employed using the deformable image registration and adaptive radiotherapy software. The validation was compared by volume-based, intensity-based, and deformation field analyses. **Results:** The use of different deformation methods greatly affected the deformable image registration accuracy from kilovoltage to megavoltage. The asymmetric transformation with the demon method was significantly better than other methods and illustrated satisfactory value for adaptive applications. The deformable image registration accuracy from kilovoltage to megavoltage showed no significant difference from the kilovoltage to kilovoltage images when using the appropriate method of registration. **Conclusions:** The choice of deformation method should be considered when applying the deformable image registration from kilovoltage to megavoltage images. The deformable image registration accuracy from kilovoltage to megavoltage revealed a good agreement in terms of intensity-based, volume-based, and deformation field analyses and showed clinically useful methods for nasopharyngeal carcinoma adaptive radiotherapy in tomotherapy applications.

Keywords

deformable image registration, MVCT, kVCT, tomotherapy, DIRART

Abbreviations

ART, adaptive radiotherapy; AsyDM, asymmetric transformation with the demon algorithm; AsyOF, asymmetric with the Horn and Schunck optical flow; DIR, deformable image registration; DIRART, deformable image registration and adaptive radiotherapy; DSC, dice similarity coefficient; DVF, deformation vector field; FFD, free-form deformation; GTV, gross tumor volume; HN, head-and-neck; ICE, inverse consistency error; kVCT, kilovoltage computed tomography; MVCT, megavoltage computed tomography;

¹ Division of Radiation Oncology, Department of Radiology, Chiang Mai University, Chiang Mai, Thailand

Corresponding Author:

Imjai Chitapanarux, Division of Radiation Oncology, Department of Radiology, Chiang Mai University, 110 Intavaroros Rd., Sripum 50200, Chiang Mai, Thailand.
Email: imjai@hotmail.com



NMI, normalized mutual information; NPC, nasopharyngeal carcinoma; OARs, organs at risk; ROI, region of interest; SymOF, symmetric with the Horn and Schunck optical flow; T_{BW} , backward transformation; T_{FW} , forward transformation

Received: May 11, 2018; Revised: October 19, 2018; Accepted: November 06, 2018.

Introduction

The treatment target and critical organs can move and become deformed during external beam radiotherapy. This movement and deformation can occur continuously during treatment. Daily image guidance using volumetric imaging kilovoltage computed tomography (kVCT) in cone-beam CT or megavoltage computed tomography (MVCT) has shown that the anatomy revealed in the originally planned CT scan often changes during treatment.¹ Several studies show the anatomy changes in patients with head-and-neck (HN) cancer during the course of the treatment, which results in dosimetric changes from the original plan. It is clear that some patients require at least 1 replan.² Castelli *et al*³ illustrated that the thickness of the neck may decrease 0.1 to 26.6 mm at the end of treatment. The parotid gland received dose average increase of 3.7 Gy (10.0 Gy maximum) from the original plan and induced of 8.2% (23.9% maximum) for the risk of xerostomia. The key step is monitoring the cumulated dose received by the deformed region of interest (ROI) to decide whether to or not to replan within the dose-guided adaptive radiotherapy (ART) strategy.⁴ To apply the ART approach routinely, it is important to follow the deformable image registration (DIR) method for creating the automatic contour and dose accumulation.¹

Currently, daily MVCT images on helical tomotherapy units (Tomotherapy Inc., Madison, Wisconsin) have become the standard guidance for most tomotherapy users, mainly for the alignment of the patient. However, the improvement of soft-tissue contrast differences is fundamentally limited in MVCT due to the number of photons used to create the image. The noise exceeds and obstructs the visibility of low-contrast objects, when the number of photons is too low.⁵ Mass energy-absorption coefficients for kV and MV photons were similar; however, absolute dose deposition per photon for MV photons was higher. Therefore, the number of MV photons required to maintain a comparable dosage for MV and kV images decreased. These conditions may degrade deformable registration accuracy due to a reduction in signal-to-noise ratio.⁶

However, Lu *et al*⁷ identified automatically localized changes in the ROI, including target organs and organs at risk (OARs) during treatment for the original kV image, and daily MVCT images with the deformable registration method using a fast intensity-based freeform. For the MVCT image, “edge-preserving smoothing” was used to improve the noise and contrast differences prior to the registration process. Moreover, Faggiano *et al*⁸ illustrated the efficiency of auto contour propagation of the parotid gland by developing the DIR methods

from kVCT to daily MVCT images with helical tomotherapy for patients with HN cancer. The applied method deformed a 3D mesh constructed by B-spline free-form deformation (FFD) to generate optimal smooth contours. Results showed that auto-contour propagation was acceptable for contouring daily MVCT images.

Nevertheless, the accuracy of DIR depends on the selection of deformation algorithms and transformation frameworks. In the registration process of MVCT, the choice is of great importance to optimize between computational efficiency and richness of description.⁹ Deformable image registration and adaptive radiotherapy (DIRART) is a software suite for DIR plus ART. The software included the large set of programs developed for image registration using MATLAB. The computational environment for radiotherapy research was applied for additional functions.¹⁰ Furthermore, DIRART offers various deformable algorithms and transformation frameworks for the DIR process.

Yeo *et al*¹¹ evaluated the accuracy of DIR for 12 algorithms implementing DIRART software. The Optical Flow algorithm provided accuracy in low-contrast regions. The demon is a well-known method for intensity-based registration. Therefore, optical flow and demon algorithms were provided in commercial software for deformable registration.^{11,12}

Our previous study gave an evaluation of DIR accuracy using various deformation models.¹³ The 4 DIR methods were applied using DIRART software with various transformation frameworks (asymmetric or symmetric transformation) and deformation algorithms (demon or optical flow algorithm). The use of symmetric transformation with the demon deformation algorithm method showed significant differences from other methods and had the worst performance in terms of volume-based criterion and inverse consistency errors (ICEs) for all the ROIs throughout the treatment. Therefore, in this study, 3 highest performing methods were selected to evaluate the effect of deformation methods on DIR accuracy from kVCT to MVCT for patients with nasopharyngeal carcinoma (NPC).

Methods

The DIR accuracy from kVCT to MVCT images was evaluated with 3 DIR methods. The DIR image procedure was divided into 3 groups. A total of 12 patients with NPC were randomly selected for carrying out the investigation. This study was approved by the institutional review board of Faculty of Medicine ChiangMai University (study code RAD-2559-03998/Research ID: 3998). All patients provided written informed consent prior to enrolment in the study.

Table 1. DIR Procedure for Source and Target Images of kV and MV in 3 DIR Methods With Different Transformations and Algorithms.

DIR Parameter	DIR Procedure	
	Source Image	Target Image
kV-kV	kVCT at first day	kVCT at 20th fraction
MV-MV	MVCT at first day	MVCT at 20th fraction
kV-MV	kVCT at first day	MVCT at 20th fraction
	DIR Method	
	Transformation	Algorithm
AsyOF	Asymmetric	Horn and Schunck optical flow
AsyDM	Asymmetric	Demons
SymOF	Symmetric	Horn and Schunck optical flow

Abbreviations: AsyDM, asymmetric transformation with demon algorithm; AsyOF, asymmetric transformation with Horn and Schunck optical flow algorithm; DIR, deformable image registration; kVCT, kilovoltage computed tomography; MVCT, megavoltage computed tomography; SymOF, symmetric transformation with Horn and Schunck optical flow algorithm.

Image Data Acquisition

The first kVCT images were acquired during the treatment planning process and the second kVCT images were taken at 20 treatment days after starting the treatment, which were acting as the source and target images, respectively. The kVCT images of all patients were acquired with a multi-slice CT scanner (Somatom; Siemens, Germany). Each slice was about 512×512 pixels with a voxel size equal to $0.976 \times 0.976 \times 3 \text{ mm}^3$ at 120 kV/106 mAs, and the average scan time was 18.13 seconds.

The first day MVCT images from the 12 patients with NPC were acquired as the source image on the same day as the kVCT image acquisition, using the helical tomotherapy unit (Tomotherapy Inc., Madison, Wisconsin). The energy for MVCT was tuned to 3.5 MeV using a matrix of 512×512 pixels with a voxel dimension of $0.763 \times 0.763 \times 4 \text{ mm}^3$. The 20th fraction MVCT was acquired as the target image for registration. Therefore, the DIR image procedure for this study was divided into 3 groups: kV-kV, MV-MV, and kV-MV images. The DIR image procedure was carried out as illustrated in Table 1.

Target Localization

For the investigation of clinical cases, the ethical approval was obtained from the institutional research committee. Prospective data from 12 patients with NPC who were treated using a helical tomotherapy treatment machine were used. All patients underwent intensity-modulated radiotherapy with a planned dose of 70 Gy delivered in 33 daily fractions. Patient positioning was ensured by using an appropriate headrest and a personalized head, neck, and shoulder mask.

The target organs and the OARs were defined by the radiation oncologists in kVCT images for treatment planning processes. The gross tumor volume (GTV) and both sides of the

parotid glands and the spinal cord were localized for investigation. The ROIs from the first kV images were transferred to the first MV images using rigid registration, with the ROIs on MVCT being approved by the radiation oncologist as source images for the MV-MV image procedure.

Regarding the image at a 20th fraction of the treatment course, the same oncologist who localized the target organs and the OARs for the tomotherapy treatment planning process also contoured the GTV, both sides of the parotid glands, and the spinal cord on the second kV images. In this study, there were 3 radiation oncologists for ROI delineation in 12 patients. Then, these were transferred to the second MV images as the reference images. These contours were compared with the automatic deformed structure generated by the DIR software.

Deformable Image Registration

Deformable image registration intends to define the corresponding volume between 2 different image sets: the source and target images. There are several DIR algorithms which can define a mapping or deformation vector field (DVF) between 2 images.¹⁴

DIRART version 1a is a popular software suite for DIR and ART, which was developed by Yang *et al.*¹⁰ There are 2 deformable registration frameworks: the regular asymmetric framework and the symmetric (inverse consistency) framework.

For transformation frameworks, regular asymmetry was found in the majority of DIR algorithms. Consequently, when changing image input sequence, the DIR does not assess inverse transformations. Analysis depends on selecting the target image; conversely, a symmetric (inverse consistency) framework assesses both forward and backward transformations (T_{BW}) simultaneously. As a result, the matching term is estimated when one image is deformed by T_{BW} and the other is deformed by forward transformation (T_{FW}).⁹

Regarding deformation algorithms, original Horn and Schunck optical flow and original demons are nonparametric deformation algorithms which describe displacement using fluid flow or deformation of a viscoelastic material based on a vector per voxel method.¹⁵ Horn and Schunck optical flow algorithm: A special kind of method is optical flow, which is used to find small deformations in temporal sequences of images. The basic hypothesis of optical flow is to consider that the intensity of a moving object is constant with time, which gives, for small displacements. These vectors can be thought of as “optical velocity” vectors showing the direction of image intensity flow.¹⁵ Original demons algorithms: The concept of the demons algorithm is that the voxels in the static or target image S act as local forces that move the voxels in the moving or source image. The moving image is iteratively deformed by applying a displacement vector u as in Equation (1):

$$u^{i+1} = \frac{(M^i - S)\nabla S}{(\nabla S)^2 + (M^i - S)^2}, \quad (1)$$

where u^{i+1} is the displacement at $i + 1$ iteration, S is the static image, M^i is the moving image at the i th iteration, and ∇S is the

gradient of the static image S . There are 2 forces in the equation: (1) the internal image gradient-based force ∇S and (2) external force $(M^i - S)$. The internal force does not change during the iterations, whereas the external force changes after each iteration. The term $(M^i - S)^2$ is added to make the deformation field computation more stable. Before the next iteration, the displacement is convolved with a Gaussian kernel, as the Gaussian convolution removes noise and improves geometric continuity.¹⁵

In this study, the DIR was performed using 3 methods with variations in the transformation frameworks (asymmetric [Asy] or symmetric [Sym] transformation) and registration algorithms (original Horn & Schunck optical flow [OF] or original demons [DM] algorithms). The 3 DIR methods, including the asymmetric with the Horn and Schunck optical flow (AsyOF), the asymmetric transformation with the demon algorithm (AsyDM), and the symmetric with the Horn and Schunck optical flow (SymOF) were employed using the DIRART software. The registration parameters used for the DIR methods are described in Table 1.

The differences in the data acquisition mechanism and photon energy between the kVCT and MVCT images make MVCT to demonstrate lower contrast than kVCT.⁷ Considering the contrast resolution and noise difference between the kVCT and the MVCT, DIRART contains a number of common image-processing tools for performing noise reduction filtering on it before the images are resampled.¹⁰ Gaussian smoothing and the kVCT to MVCT intensity remapping are applied to the MVCT image prior to the deformable registration process.

These frameworks support multiresolution (to sequentially register the 2 images from the lower resolutions to the higher resolutions.) DIRART implemented the multigrid and multiple-pass approaches. Multigrid is an approach to down-sample the images and to perform image registration sequentially from low resolution to high resolution. After registration is finished in an image resolution stage, the result will be used as the initial condition for the next image resolution stage. Multiple-pass approach is similar to multigrid approach. The concept is to apply registration in multiple times on the same image resolution stage. The registration can be repeated to perform in a new pass based on the result of the previous pass due to the result of image registration in 1 computation is often not good enough.¹⁰

To define the DIR performance for each algorithm, several parameters were adjusted. For the optical flow algorithm, 4 multigrids were used ($n = 1, 2, 3,$ and 4) and the number of passes was 6. For the demon algorithm, 4 multigrids were used and the number of passes was between 2 and 6. Resampling at finer resolutions after coarser stage approaches with a higher number of passes to gain the concordance with the target image.¹⁶

Validation Technique

The validation technique with respect to the volume-based criterion, the intensity-based criterion, and deformation field

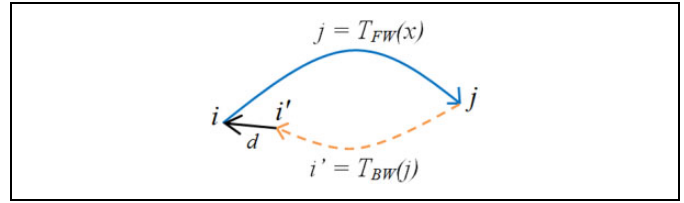


Figure 1. Schematization of the inverse consistent error¹⁸: $d = \text{ICE} = \|I - i'\|$. ICE indicates inverse consistency; T_{BW} , backward transformation; T_{FW} , forward transformation.

analysis was used to evaluate the registration accuracy in 3 image procedures with different DIR methods.

For the volume-based criterion, the overlapping volume of the structure created by the radiation oncologist and the DIRART-deformed contours of the deformation shapes were assessed. The most common overlap metric was the Dice similarity coefficient (DSC).¹⁵ The DSC is the metric which computes the number of pixels that overlap between the 2 volumes as in Equation (2), which is defined as 2 times the overlap of A' and B , divided by the sum of the volume of A' and B as shown below:

$$\text{DSC} = 2(A' \cap B)/(A' + B). \quad (2)$$

If the images have no overlapping pixels, then the DSC is 0; as the contours become identical, the DSC approaches a value close to 1.¹⁵ Goldberg-Zimring *et al*¹⁷ proposed that the acceptable volume matching score should be higher than 70% (DSC of 0.7) for the ART application.

For the intensity-based criterion, the normalized mutual information (NMI) was used to ensure image-matching quality. The NMI can range between 0 and 2, and NMI values greater than 1 typically represent a good match between images.¹⁷

For deformation field analysis, the ICE was used to ensure that the transformations were physically plausible. The ICE assesses the degree of consistency between forward and backward frameworks. The T_{FW} maps from point i to j , whereas the T_{BW} maps the point j to i' . The distance between i and i' consists of the ICE: $\text{ICE} = \|I - i'\|$ (Figure 1).¹⁸ The optimal transformation is defined by minimizing d (distance). The composition yields 0, if the deformation maps are true inverses.¹⁹

The normality of the variable distributions was verified for DSC, NMI, and ICE using the Shapiro test for all the image procedures. An analysis of variance was performed for normal variable distributions, and the Kruskal–Wallis test was performed for nonparametric statistic using version 17 of the SPSS statistical program to assess the impact of each DIR method.

Results

Effect of DIR Methods on the Accuracy on kV and MV Images

The results for the DIR accuracy were consistent in terms of the volume-based criterion, DSC, the intensity-based criterion,

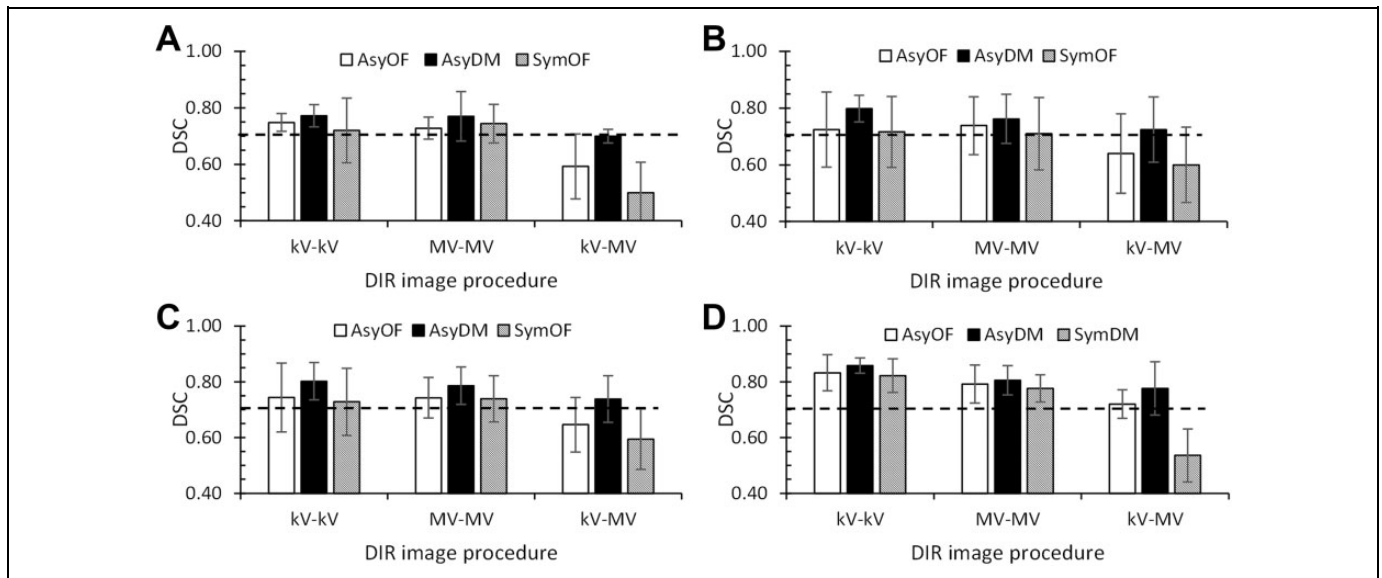


Figure 2. Histogram of the Dice similarity coefficients (DSCs) of (A) gross tumor volume (GTV), (B) left parotid, (C) right parotid, and (D) spinal cord for kilovoltage computed tomography (kVCT) and megavoltage computed tomography (MVCT) image procedures in kV-kV, MV-MV, and kV-MV by asymmetric with the Horn and Schunck optical flow (AsyOF), asymmetric transformation with demon algorithm (AsyDM), and symmetric with the Horn and Schunck optical flow (SymOF) deformable image registration (DIR) methods.

NMI, and the deformation field analysis, ICE. Figure 2A to D illustrates the histogram of the mean DSC values for all of the ROIs by the 3 DIR methods. The AsyDM method showed the best agreement with DSC values greater than 0.7 for all the ROIs in the 3 groups. Moreover, for the kV-MV image, the AsyDM was the only method that still shows a DSC greater than 0.7 by generating mean DSC values of 0.700 (0.07), 0.738 (0.08), 0.724 (0.11), and 0.776 (0.10) for the GTV, left parotid, right parotid, and spinal cord, respectively. On the other hand, the SymOF method showed the lowest scores with mean DSC values of 0.500 (0.11), 0.600 (0.13), 0.594 (0.11), and 0.536 (0.10) for the GTV, left parotid, right parotid, and spinal cord, respectively.

Figure 3 illustrates the automatic deformed contour of the right parotid gland in 1 NPC case from the 3 DIR methods in the 3 groups of the DIR image procedures. For the kV-kV and MV-MV image procedures, the automatic deformations of the right parotid (red line) were shown similarly in all 3 DIR methods. On the other hand, for the kV-MV image procedure, the AsyDM methods showed the best agreement of automatic deformation and reference contour with distinctive performance. The AsyOF and SymOF methods demonstrated good performance only in the kV-kV and MV-MV images and showed poor agreement in the kV-MV images.

For the intensity-based criterion and the deformation field analysis, the results of the DIR accuracy were concordant in terms of NMI and ICE, as demonstrated in Figure 4A and B, respectively. The best performance was delivered by the AsyDM method, with the highest mean NMI values and lowest ICE values in all the image procedures. Conversely, the SymOF method showed the worst agreement, with the lowest mean NMI values and highest ICE values for the 3 image procedures.

The validation values of the DIR accuracy are shown in Table 2. For the kV-kV image procedure, the use of various DIR methods was not significantly different in the volume-based analysis with $P = .545, .601, .517,$ and $.629$ for the GTV, right parotid, left parotid, and spinal cord, respectively. Similar to the MV-MV image procedure, the various DIR methods were not significantly different in the volume-based analysis with $P = .545, .601, .517,$ and $.629$ for the GTV, right parotid, left parotid, and spinal cord, respectively. However, there were significant differences in ICE, with P values of $.004$ (kV-kV) and $.001$ (MV-MV). In contrast, for the kV-MV image procedure, there were significant differences when using the different DIR method, with $P = .037, .014, .041, .004,$ and $.043$ for the GTV, right parotid, left parotid, spinal cord, and ICE, respectively. The AsyDM method showed the best agreement with a mean DSC greater than 0.7 for the all ROIs, the highest NMI, and the lowest ICE.

Evaluated DIR in 3 Image Procedures

Regarding the kV-kV, MV-MV, and kV-MV image procedures, the DIR accuracy from the 3 image procedures was not significantly different when using the AsyDM method, with $P = .080$ (DSC), $.740$ (NMI), and $.057$ (ICE). This result demonstrated that the DIR accuracy on the kV images was not significantly different from that of the MV images. However, when applying the DIR with the AsyOF and SymOF methods, the DSC value of kV-MV was significantly lower, with $P = .002$ (AsyOF) and $.000$ (SymOF). Conversely, the NMI values were not significantly different in the kV-kV, MV-MV, and kV-MV images for all 3 methods, with $P = .542$ (AsyOF), $.740$ (AsyDM), and $.835$ (SymOF). Similar to the ICE, all

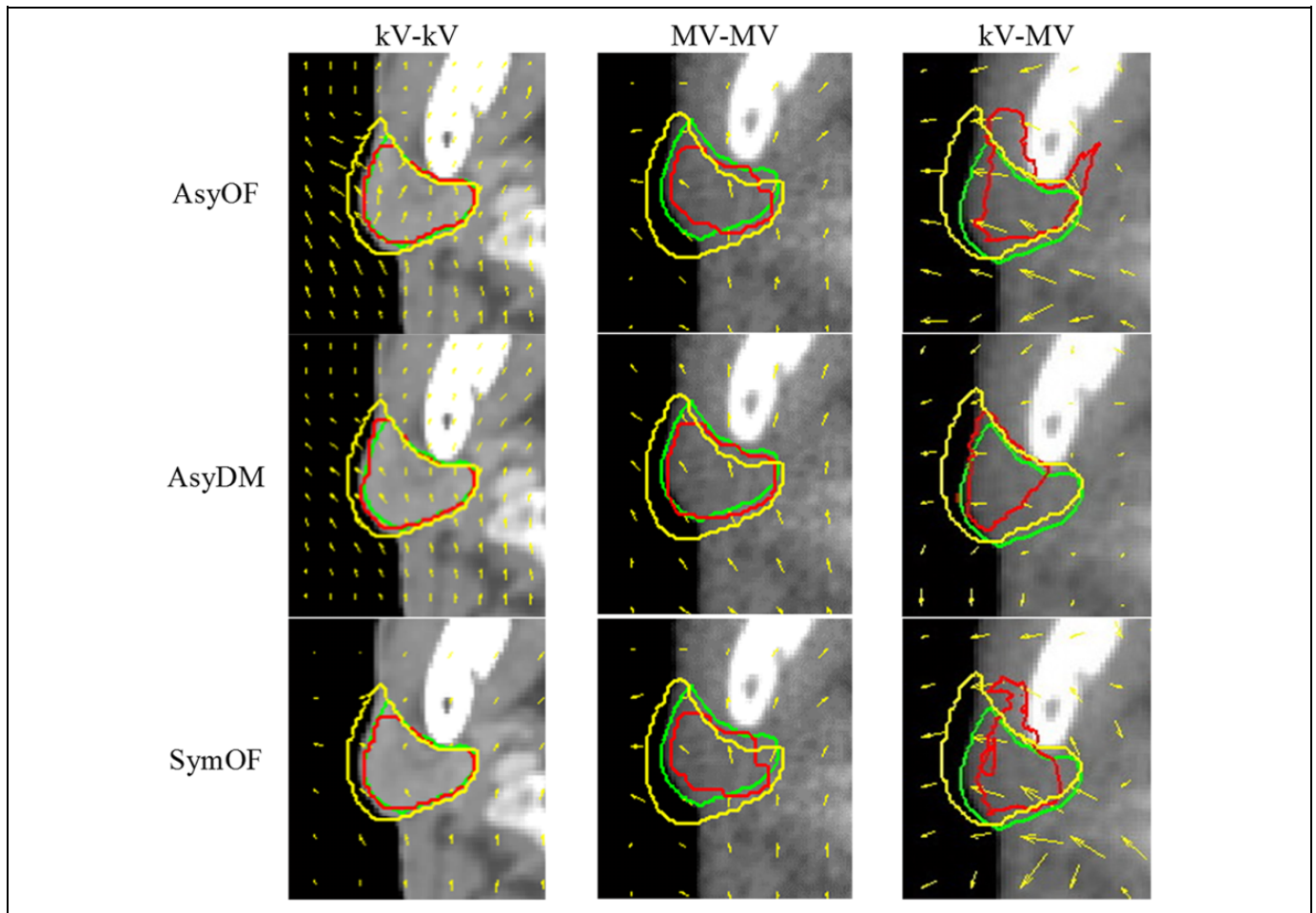


Figure 3. The automatic deformed images of the right parotid gland (red) deformed from the original contour (yellow), in comparison with the reference contour (green) in 1 nasopharyngeal carcinoma (NPC) case for kilovoltage computed tomography (kVCT) and megavoltage computed tomography (MVCT) image procedures in kV-kV, MV-MV, and kV-MV by asymmetric with optical flow (AsyOF), asymmetric transformation with the demons algorithm (AsyDM), and symmetric with the Horn and Schunck optical flow (SymOF) deformable image registration (DIR) methods.

3 methods were not significantly different in the kV-kV, MV-MV, and kV-MV image procedures, with $P = .493$ (AsyOF), $.057$ (AsyDM), and $.240$ (SymOF).

Discussion

Figure 2 demonstrates the overlapping volume analysis of the target organs and OARs with the DSC value. The best DIR method for all the DIR image procedures was the AsyDM method, with average DSC values of 0.808 (0.03), 0.781 (0.02), and 0.735 (0.03) for the kV-kV, MV-MV, and kV-MV images, respectively. Nobnop *et al*¹³ revealed that the AsyDM method showed the best performance with MVCT to MVCT deformable registration with the highest average of DSC = 0.804 (0.07). Moreover, the DSC values were concordant with previous studies. Rigaud *et al*⁴ assessed results for 10 DIR approaches by variation in registration algorithms (demons or B-spline FFD), preprocessing, and similarity metrics. The most accurate DIR method was the demon for

both mutual information metrics and filtered CTs. Mean values of DSC for the parotid gland were 0.75 for demons with original CTs using the mean square error metric. Results showed that selecting image preprocessing for the metric was important as the registration method. Varadhan *et al*¹⁹ illustrated a framework which analyzed the performance of HN study sets using 2 DIR algorithms (B-spline and diffeomorphic demons) with 2 directions (forward and inverse). The diffeomorphic demons method gave a mean value of DSC at 0.74. This method offered clinical acceptability for NPC ART.

With AsyDM, the normal organs were more accurately deformed than the target structure, and the mean DSC values for the GTV were 0.772 (0.07; kV-kV), 0.770 (0.09; MV-MV), and 0.700 (0.07; kV-MV). The average DSC values for the all OARs were 0.819 (0.03; kV-kV), 0.785 (0.02; MV-MV), and 0.746 (0.02; kV-MV). Hardcastle *et al*¹ demonstrated good agreement between the automatically deform contour and the expert-drawn ROIs. Approximately 94% of all the ROIs generated using DIR could be scored as clinically useful, requiring

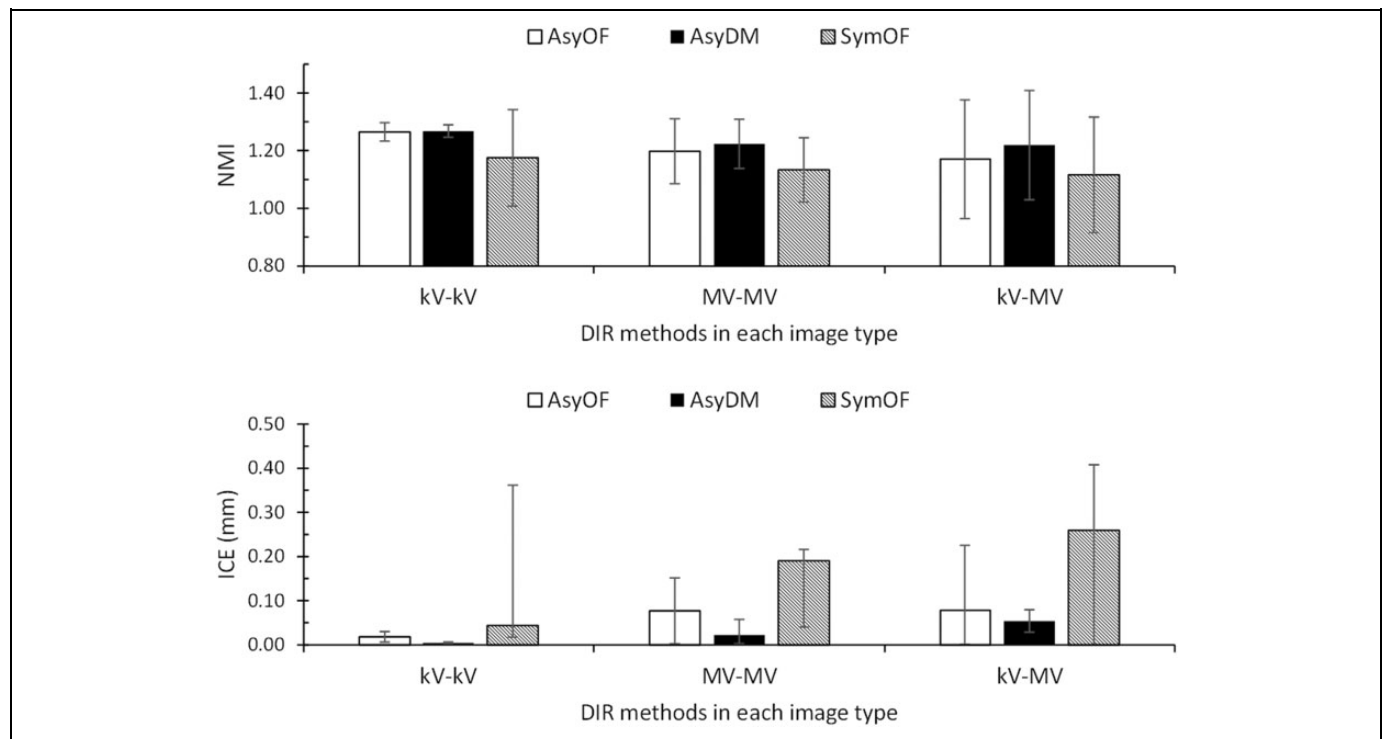


Figure 4. Histogram of the (A) normalized mutual information (NMI) and (B) inverse consistency error (ICE) for kilovoltage computed tomography (kVCT) and megavoltage computed tomography (MVCT) image procedures in kV-kV, MV-MV, and kV-MV by asymmetric with optical flow (AsyOF), asymmetric transformation with the demon algorithm (AsyDM), and symmetric with the Horn and Schunck optical flow (SymOF) deformable image registration (DIR) methods.

Table 2. Comparison of Mean Values of DSC, NMI, and ICE by 3 DIR Methods for Different Image Procedures.

DIR Image Procedures	Validation Techniques	DIR Methods, Mean (SD)			P Value ^a
		AsyOF, mean (SD)	AsyDM, mean (SD)	SymOF, mean (SD)	
kV-kV	DSC				
	- GTV	0.748 (0.03)	0.772 (0.07)	0.720 (0.06)	.545 ^b
	- Right parotid	0.744 (0.12)	0.802 (0.07)	0.728 (0.12)	.601 ^b
	- Left parotid	0.724 (0.13)	0.798 (0.05)	0.716 (0.12)	.517 ^b
	- Spinal cord	0.832 (0.06)	0.858 (0.03)	0.822 (0.06)	.629 ^b
	NMI	1.265 (0.03)	1.268 (0.02)	1.175 (0.17)	.353 ^b
	ICE	0.018 (0.01)	0.004 (0.00)	0.043 (0.03)	.004 ^c
MV-MV	DSC				
	- GTV	0.728 (0.04)	0.770 (0.09)	0.744 (0.02)	.592 ^b
	- Right parotid	0.743 (0.07)	0.786 (0.07)	0.739 (0.08)	.275 ^b
	- Left parotid	0.738 (0.10)	0.762 (0.09)	0.710 (0.13)	.530 ^b
	- Spinal cord	0.792 (0.07)	0.806 (0.05)	0.776 (0.05)	.763 ^b
	NMI	1.198 (0.11)	1.224 (0.09)	1.133 (0.11)	.127 ^b
	ICE	0.077 (0.07)	0.022 (0.04)	0.190 (0.15)	.001 ^c
kV-MV	DSC				
	- GTV	0.593 (0.70)	0.700 (0.07)	0.500 (0.11)	.037 ^b
	- Right parotid	0.646 (0.10)	0.738 (0.08)	0.594 (0.11)	.014 ^b
	- Left parotid	0.640 (0.14)	0.724 (0.11)	0.600 (0.13)	.041 ^b
	- Spinal cord	0.720 (0.05)	0.776 (0.10)	0.536 (0.10)	.004 ^b
	NMI	1.171 (0.21)	1.219 (0.19)	1.116 (0.20)	.070 ^c
	ICE	0.078 (0.15)	0.054 (0.03)	0.260 (0.32)	.043 ^c

Abbreviations: ANOVA, analysis of variance; AsyDM, asymmetric transformation with demon algorithm; AsyOF, asymmetric transformation with Horn and Schunck optical flow algorithm; DIR, deformable image registration; DSC, dice similarity coefficient; GTV, gross tumor volume; ICE, inverse consistency error; NMI, normalized mutual information; SymOF, symmetric transformation with Horn and Schunck optical flow algorithm.

^aStatistical tests.

^bANOVA.

^cNonparametric Kruskal–Wallis test.

minimal or no edits. Nevertheless, 27% (12/44) of the GTVs required major edits. The results demonstrate that the use of different deformation models and different ROIs affects the accuracy of the DIR.

Normally, kVCT images have more accuracy in cases where the DIR is generated by high contrast. However, the kV-kV images for 2 patients with NPC showed inferior results due to dental fillings. For the kVCT images, the metal (much higher Z) increased the photoelectric attenuation and caused streaking artifacts; however, streak artifacts were minimal in the MVCT images.⁶ Artifact images decrease the accuracy of the DIR. The mean DSC values of both parotid glands in the patients with dental fillings were 0.651 (0.126; left) and 0.666 (0.116; right) in the kV-kV images.

Regarding the deformation field analysis, Rogelj and Kovacic²⁰ demonstrate the advantages of symmetric registration for deformation analysis in terms of ICE. This measures the similarity between the images in both registration directions in order to gather more information about the image transformation. The results show that the symmetric approach improves both the registration consistency and the registration correctness. Moreover, Lourenço¹⁸ assessed and evaluated different methods to compute the inverse of a B-Spline transformation for 5 patients with HN cancer. The results show that the average ICE was 1.755 mm for asymmetric and 0.462 mm for symmetric transformations. Conversely, this study found that most asymmetric transformations showed better performance than symmetric transformations. The average ICE for kV-MV images was 0.078 (0.15; AsyOF), 0.054 (0.03; AsyDM), and 0.260 (0.32; SymOF). The asymmetric transformation's superior results were due to the process of generating the inverse DVF. The inverse DVF was generated from the same DVF direction to analyze the ICE. This cause of the errors between the 2 directions (DVF and inverse DVF) in asymmetric transformation is lower than the symmetric transformation. However, a limitation of asymmetric transformation is that the registration error depends on the selection of the registration direction. The first images should be the source image and the second images should be used as the target image. Changing the order of the input images affected the results.⁹

This study revealed that the DIR accuracy in the single modality can perform better than the DIR in multimodality images. When the DIR from kV-MV is considered, the DIR application method should be taken into account. For practical application, kVCTs were set as the source image, and tomotherapy image-guided modality MVCTs were set as the target image. This study showed no significant differences from kV-kV registration when the AsyDM method was used. The results revealed that MV-MV performed better than kV-MV. The use of the first day MVCT image as the source image was the one of the choices for achieving superior DIR results because the use of DIR methods was not extremely affected by the MV-MV image procedure.

In this study, the volume matching from the AsyDM method performed satisfactorily for the adaptive application, with DSC values greater than 0.7 for all image procedures. The results

demonstrated good agreement in terms of intensity-based, volume-based, and deformation field analyses and showed clinically useful DIR methods on MVCT images for NPC ART in tomotherapy applications.

Acknowledgments

The authors thank the staff of the Division of Radiation Oncology, Faculty of Medicine, Chiang Mai University, for supporting this study.

Declaration of Conflicting Interests

The author(s) declared no potential conflicts of interest with respect to the research, authorship, and/or publication of this article.

Funding

The author(s) received no financial support for the research, authorship, and/or publication of this article.

ORCID iD

Wannapha Nobnop, PhD  <https://orcid.org/0000-0002-5266-2845>

References

1. Hardcastle N, Tomé WA, Cannon DM, et al. A multi-institution evaluation of deformable image registration algorithms for automatic organ delineation in adaptive head and neck radiotherapy. *Radiat Oncol J*. 2012;7:1-7. doi:10.1186/1748-717X-7-90.
2. Veiga C, McClelland J, Moinuddin S, et al. Toward adaptive radiotherapy for head and neck patients: feasibility study on using CT-to-CBCT deformable registration for “dose of the day” calculations. *Med Phys*. 2014;41(3):031703. doi:10.1118/1.4864240.
3. Castelli J, Simon A, Louvel G, et al. Impact of head and neck cancer adaptive radiotherapy to spare the parotid glands and decrease the risk of xerostomia. *Radiat Oncol J*. 2015;10:6. doi:10.1186/s13014-014-0318-z.
4. Rigaud B, Antoine S, Castelli J, et al. Evaluation of deformable image registration methods for dose monitoring in head and neck radiotherapy. *Biomed Res Int*. 2015;2015:726268. doi:10.1155/2015/726268.
5. Keller H, Glass M, Hinderer R, et al. Monte Carlo study of a highly efficient gas ionization detector for megavoltage imaging and image-guided radiotherapy. *Med Phys*. 2002;29(2):165-175. doi:10.1118/1.1445414.
6. Ruchala KJ, Olivera GH, Schloesser EA, Mackie TR. Megavoltage CT on a tomotherapy system. *Phys Med Biol*. 1999;44(10):2597-2621. doi:10.1088/0031-9155/44/10/316.
7. Lu W, Olivera GH, Chen Q, et al. Deformable registration of the planning image (kVCT) and the daily images (MVCT) for adaptive radiation therapy. *Phys Med Biol*. 2006;51(17):4357-4374. doi:10.1088/0031-9155/51/17/015.
8. Faggiano E, Fiorino C, Scalco E, et al. An automatic contour propagation method to follow parotid gland deformation during head-and-neck cancer tomotherapy. *Phys Med Biol*. 2011;56(3):775-791. doi:10.1088/0031-9155/56/3/015.
9. Sotiras A, Davatzikos C, Paragios N. Deformable medical image registration: a survey. *IEEE Trans Med Imaging* 2013;32(7):1153-1190.

10. Yang D, Brame S, El Naqa I, et al. Technical note: DIRART—a software suite for deformable image registration and adaptive radiotherapy research. *Med Phys*. 2011;38(1):71-77. doi:10.1118/1.3521468.
11. Yeo U, Supple J, Taylor M, Smith R, Kron T, Franich R. Performance of 12 DIR algorithms in low-contrast regions for mass and density conserving deformation. *Med Phys*. 2013;40(10):101701. doi:10.1118/1.4819945.
12. Weistrand O, Svensson S. The ANACONDA algorithms for deformable image registration in radiotherapy. *Med Phys*. 2015;42(1):40-53.
13. Nobnop W, Chitapanarux I, Neamin H, Wanwilairat S, Lorvidhaya V, Sanghangthum T. Evaluation of deformable image registration (DIR) methods for dose accumulation in nasopharyngeal cancer patients during radiotherapy. *Radiol Oncol*. 2017;51(4):438-446. doi:10.1515/raon-2017-0033.
14. Bender ET, Hardcastle N, Tome WA. On the dosimetric effect and reduction of inverse consistency and transitivity errors in deformable image registration for dose accumulation. *Med Phys*. 2012;39(1):272-280.
15. Kristy KB. *Image Processing in Radiation Therapy*. New York: Taylor & Francis Group; 2013.
16. Bissonnette JP, Purdie TG. Cone-beam computed tomographic image guidance for lung cancer radiation therapy. *Int J Radiat Oncol Biol Phys*. 2009;73:927-934. doi:10.1016/j.ijrobp.2008.08.059.
17. Goldberg-Zimring D, Talos IF, Bhagwat JG, Haker SJ, Black PM, Zou KH. Statistical validation of brain tumor shape approximation via spherical harmonics for image-guided neurosurgery. *Acad Radiol*. 2005;12(4):459-466. doi:10.1120/jacmp.v14i1.4066.
18. Lourenço A. *Deformable Registration, Dose Remapping and Summation for Head and Neck Adaptive Radiotherapy Applications*. Lisbon, Portugal; University of Lisbon; 2013.
19. Varadhan R, Karangelis G, Krishnan K, Hui S. A framework for deformable image registration validation in radiotherapy clinical applications. *J Appl Clin Med Phys*. 2013;14(1):4066. doi:10.1120/jacmp.v14i1.4066.
20. Rogelj P, Kovacic S. Symmetric image registration. *Med Image Anal*. 2006;10(3):484-493. doi:10.1016/j.media.2005.03.003.